

# Trade-off Between Optimal Efficiency and Envelope Correlation Coefficient for Antenna Clusters

Vojtech Neuman, Miloslav Capek, *Senior Member, IEEE*, Lukas Jelinek, Anu Lehtovuori, and Ville Viikari, *Senior Member, IEEE*

**Abstract**—This paper introduces a theory for assessing and optimizing the multiple-input-multiple-output performance of multi-port cluster antennas in terms of efficiency, channel correlation, and power distribution. A method based on a convex optimization of feeding coefficients is extended with additional constraints allowing the user to control a ratio between the power radiated by the clusters. The formulation of the problem makes it possible to simultaneously optimize total efficiency and channel correlation with a fixed ratio between power radiated by the clusters, thus examining a trade-off between these parameters. It is shown that channel correlation, total efficiency, and allocation of radiated power are mutually conflicting parameters. The trade-offs are shown and discussed. The theory is demonstrated on a four-element antenna array and on a mobile terminal antenna.

**Index Terms**—Antennas, electromagnetic theory, feeding optimization, multiple-input-multiple-output, mutual coupling, convex optimization.

## I. INTRODUCTION

**M**ULTIPLE-INPUT-MULTIPLE-OUTPUT (MIMO) technology has proven its utility in wireless communication in increasing data throughput and coverage while mitigating signal fading due to multipath propagation [1]. All contemporary wireless standards utilize MIMO [2], and this trend is expected to continue [3], [4]. Of high priority is the implementation of MIMO technology for mobile devices at sub-6 GHz frequency bands [2]. Though narrow bands at this frequency range cannot offer data rates as high as millimeter-wave frequencies, they still have an advantage in robustness against environmental influences and free space loss [5], [6]. The small electric size of user devices in these frequency bands nevertheless significantly degrades their efficiency and channel correlation performance, two key parameters affecting MIMO system performance [1], [7].

When speaking of efficiency we refer to an antenna's ability to transform incoming guided power into radiated power [8]. In the current state of the art, approaches exist for efficiency enhancement [9], [10]. Nevertheless, they solely deal with the

efficiencies of individual channels, *i.e.*, one antenna element is fed, and the rest of the elements are terminated into the given impedance [11]. The efficiency is evaluated, measured, or optimized only under this feeding scenario. Although this method is simple, when the system is not well-isolated, an input impedance of a given port heavily depends on the feeding of other ports of a multi-port system. The efficiencies derived in this way may not reflect the realized efficiencies under active (simultaneous) feeding of all ports. The method introduced in this paper enables the versatile design of a multi-antenna system and avoids above mentioned issues by considering only the total efficiency of the whole radiating system which means that the correct input impedance of all ports concerning chosen feeding is taken into account.

Channel correlation is closely associated with mutual coupling between antenna ports [7], [12]. Several approaches were introduced to reduce it [9], [13], *e.g.*, defective ground surfaces [14]–[16], electromagnetic band-gap structures [13], decoupling networks [17], utilization of characteristic modes theory [18]–[20], or employment of point symmetries [21], [22]. These techniques have proven their ability to reduce mutual coupling. However, they cannot optimize the system's total efficiency simultaneously.

The method applied in this paper is based on grouping more antenna elements into so-called antenna clusters [23]. The mutual coupling between elements within one cluster is employed to increase its performance. The antenna cluster consists of multiple elements, each having its ports and proper feeding coefficients at every frequency to ensure optimal performance. A distributed transmitter supports this operation principle [24]. Replicating antenna clusters within the design region leads to MIMO functionality [25]. Although mutual coupling is beneficial between elements of one antenna cluster, it is still a potential issue in the MIMO system [25], *i.e.*, between different clusters.

This paper aims to introduce the simultaneous optimization of total efficiency and channel correlation, constrained by a user-defined allocation of power radiated by the clusters. This is achieved by employing antenna cluster feeding optimization [25], [26] supplemented by additional constraints for controlling channels radiating power and power interfering between channels. The optimization is solely based on the utilization of a matrix description. This work additionally proposes a theory of power ratios where the radiated power is divided into individual components describing the power composition. The above allows the analysis of a trade-off between efficiency, radiated power by channels, and channel

Manuscript received May 3, 2023; revised May 3, 2023. This work was supported by the Czech Science Foundation under project No. 21-19025M and by the Czech Technical University in Prague under project SGS22/162/OHK3/3T/13.

V. Neuman, M. Capek and L. Jelinek are with the Czech Technical University in Prague, Prague, Czech Republic (e-mails: {vojtech.neuman; miloslav.capek; lukas.jelinek}@fel.cvut.cz).

A. Lehtovuori and V. Viikari are with the Aalto University, Espoo, Finland (e-mails: {anu.lehtovuori; ville.viikari}@aalto.fi).

Color versions of one or more of the figures in this paper are available online at <http://ieeexplore.ieee.org>

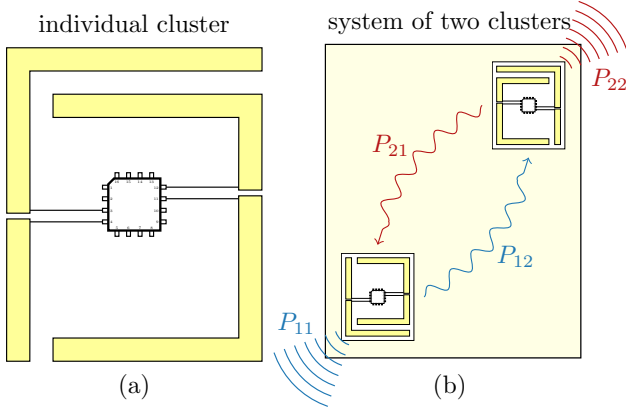


Fig. 1. Illustration of an antenna cluster. The indicated integrated circuit represents a distributed transceiver. (a) Multi-port antenna forming an antenna cluster (two feeding ports, two radiating elements). (b) Two antenna clusters forming an antenna system. The wavy curves and arrows depict self and mutual radiated powers.

correlation.

The organization of this paper is as follows. Section II introduces the mathematical tools used. The modified optimization procedure is described in Sec. III, and its application is shown in Sec. IV and Sec. V. The paper concludes in Sec. VI. Appendices A and B reviews the theoretical background, and Appendices C and D deal with further aspects of the developed theory.

## II. RADIATION OF ANTENNA CLUSTERS

An example of an antenna cluster is shown in Fig. 1(a). Multiple antenna clusters establish a radiating system (MIMO), see Fig. 1(b), where two antenna clusters form two individual communication channels.

The  $N$  ports of the radiating body are divided into  $M$  antenna clusters, where the  $m$ -th antenna cluster has  $N_m$  assigned ports

$$N = \sum_{m=1}^M N_m. \quad (1)$$

The number  $M$  also defines the order of the MIMO used [1].

The radiating system is fully described with its admittance matrix  $\mathbf{y} \in \mathbb{C}^{N \times N}$ , see Appendix A, which, together with port voltages, calculate cycle mean power

$$\frac{1}{2} \mathbf{v}^H \mathbf{y} \mathbf{v} = \frac{1}{2} \mathbf{v}^H \mathbf{g}_0 \mathbf{v} + \frac{i}{2} \mathbf{v}^H \mathbf{b}_0 \mathbf{v} = P + iP_{\text{react}}, \quad (2)$$

where  $\mathbf{g}_0$  is the port radiation matrix,  $\mathbf{b}_0$  is the port susceptance matrix,  $P$  denotes radiated power,  $P_{\text{react}}$  represents reactive power and  $\mathbf{v} \in \mathbb{C}^{N \times 1}$  aggregates feeding voltages connected to the antenna ports. Considering the far-field correlation, see Appendix B, the port radiation matrix  $\mathbf{g}_0$  is the

operator of primary interest<sup>1</sup>. Individual elements of radiation matrix  $\mathbf{g}_0$  are grouped into blocks as

$$\mathbf{g}_0 = \begin{bmatrix} \mathbf{g}_{0,11} & \cdots & \mathbf{g}_{0,1M} \\ \vdots & \ddots & \vdots \\ \mathbf{g}_{0,M1} & \cdots & \mathbf{g}_{0,MM} \end{bmatrix}, \quad (3)$$

with  $\mathbf{g}_{0,mm} \in \mathbb{C}^{N_m \times N_m}$  describing the interaction within the  $m$ -th cluster and  $\mathbf{g}_{0,mn} \in \mathbb{C}^{N_m \times N_n}$  considering interactions between the  $m$ -th and  $n$ -th cluster. The radiation matrix is hermitian

$$\mathbf{g}_{0,nm} = \mathbf{g}_{0,mn}^H. \quad (4)$$

For a simplification of the matrix description, the indexing operators  $\mathbf{C}_m \in \mathbb{B}^{N \times N_m}$  are introduced as

$$C_{m,kl} = \begin{cases} 1 & \text{the } k\text{-th port is the } m\text{-th cluster } l\text{-th port,} \\ 0 & \text{otherwise.} \end{cases} \quad (5)$$

Applying this operator from both sides on the port-mode radiation matrix gives

$$\mathbf{g}_{0,mn} = \mathbf{C}_m^H \mathbf{g}_0 \mathbf{C}_n. \quad (6)$$

Using the combination of  $\mathbf{C}_m \mathbf{C}_m^H$  on the same group of operators provides a matrix that reads

$$\tilde{\mathbf{g}}_{0,mn} = \mathbf{C}_m \mathbf{C}_m^H \mathbf{g}_0 \mathbf{C}_n \mathbf{C}_n^H = \begin{bmatrix} \mathbf{0} & \cdots & \mathbf{0} \\ \vdots & \mathbf{g}_{0,mn} & \vdots \\ \mathbf{0} & \cdots & \mathbf{0} \end{bmatrix}. \quad (7)$$

Those two principles are frequently used in the following.

The feeding of an antenna is also partitioned into blocks, each representing a feeding vector of a particular cluster

$$\mathbf{v} = [\mathbf{v}_1^T \quad \cdots \quad \mathbf{v}_M^T]^T, \quad (8)$$

where  $\mathbf{v} \in \mathbb{C}^{N \times 1}$  contains vectors  $\mathbf{v}_m \in \mathbb{C}^{N_m \times 1}$  corresponding to the  $m$ -th cluster feeding.

The radiated power consists of terms

$$P_{mn} = \frac{1}{2} \mathbf{v}^H \mathbf{C}_m \mathbf{C}_m^H \mathbf{g}_0 \mathbf{C}_n \mathbf{C}_n^H \mathbf{v} = \frac{1}{2} \mathbf{v}_m^H \mathbf{g}_{0,mn} \mathbf{v}_n, \quad (9)$$

where  $m = n$  represents self terms, and  $m \neq n$  represents interaction terms. Summing all contributions gives the total radiated power

$$P = \frac{1}{2} \sum_m \mathbf{v}_m^H \mathbf{g}_{0,mm} \mathbf{v}_m + \frac{1}{2} \sum_m \sum_{n \neq m} \mathbf{v}_m^H \mathbf{g}_{0,mn} \mathbf{v}_n. \quad (10)$$

Notice that only total radiated power  $P$  in (10) has a clear physical meaning. The separation into generally complex-valued terms (9) is only used to exploit their mathematical properties for the optimization procedure discussed in Sec. III. It is nevertheless worth mentioning that power terms  $P_{mn}$  are directly related to the far-field correlation coefficient, see (35) in Appendix B.

<sup>1</sup>Although the lossless antennas are used for simplicity, lossy cases can be included without any major modification of the theory, see Appendix A.

Dividing relation (10) by total radiated power  $P$  leads to power ratios  $\alpha_{mn}$

$$1 = \sum_m \alpha_{mm} + \sum_m \sum_{n \neq m} \alpha_{mn} = \sum_m \alpha_{mm} + \sum_m \sum_{n > m} \beta_{mn}, \quad (11)$$

where  $\alpha_{mn} = P_{mn}/P$  and  $\beta_{mn} = \alpha_{mn} + \alpha_{nm}$ . Power ratios  $\alpha_{mn}$  with  $m \neq n$  have an imaginary part, for which  $\gamma_{mn}$  is defined as

$$\gamma_{mn} = i(\alpha_{mn} - \alpha_{nm}). \quad (12)$$

The power ratios are used in the optimization to control the composition of the radiated power. The self-term power ratios  $\alpha_{mm}$  control useful radiated power, and  $\beta_{mn}, \gamma_{mn}$  are used to limit the mutual radiated power. More details are given in Appendices C and D.

### III. OPTIMIZATION PROBLEM AND CONSTRAINTS

The trade-off between far-field correlation, total efficiency, and power allocation is formulated in this section, starting with simpler sub-problems.

The optimization problem for maximum total efficiency  $\eta$  reads

$$\begin{aligned} & \underset{\mathbf{v}}{\text{maximize}} && P \\ & \text{subject to} && P_{\text{in}} = 1, \end{aligned} \quad (13)$$

and it can be solved as a generalized eigenvalue problem [26]. This formulation delimits the highest total efficiency achieved with a given set of ports. To constrain optimization, the power delivered to the antennas is fixed. Depending on the knowledge of the feeding system, the delivered power can be determined as available power [27], [28] or input power [29], see Appendix A. The problem (13) is unable to distinguish individual channels. Therefore, a modification in the form of additional constraints is required.

Observing the formula for the far-field correlation (35), it is clear that the term in its numerator should be minimized. The terms of form  $P_{mn}$  with  $m \neq n$  are generally complex and unsuitable for convex solvers. Thus real mutual radiated power  $P_{mn,\text{real}}$  is introduced and defines a constraint on mutual radiated power

$$P_{mn,\text{real}} = P_{mn} + P_{nm} = \beta_{mn}P. \quad (14)$$

where  $\beta_{mn}$  is the power ratio from (11) the value of which is set by the user during optimization.

Constraint (14) deals only with the real part of the correlation coefficient (35). The imaginary part also has to be suppressed. A constraint on imaginary mutual power  $P_{mn,\text{imag}}$  reads

$$P_{mn,\text{imag}} = i(P_{mn} - P_{nm}) = \gamma_{mn}P \quad (15)$$

where  $\gamma_{mn}$  is used in a similar manner as  $\beta_{mn}$ .

The trivial solution for zeroing channel correlation is to set either  $\mathbf{v}_m$  or  $\mathbf{v}_n$  to zero vector. Nevertheless, this would lead to a situation in which  $P_{mm}$  or  $P_{nn}$  equals zero. Such a scenario is unacceptable since it disables one of the clusters. Hence,

another set of constraints must be defined. To that point, self-radiated powers  $P_{mm}$  are constrained via

$$P_{mm} = \alpha_{mm}P, \quad (16)$$

stating that the channel radiates a user-defined ratio  $\alpha_{mm}$  of total radiated power.

Considering the constraints defined above, the modified optimization problem reads

$$\begin{aligned} & \underset{\mathbf{v}}{\text{maximize}} && P \\ & \text{subject to} && P_{\text{in}} = 1, \\ & && P_{mm} = \alpha_{mm}P, \forall m \\ & && P_{mn,\text{real}} = \beta_{mn}P, \forall m, n \wedge m \neq n, \\ & && P_{mn,\text{imag}} = \gamma_{mn}P, \forall m, n \wedge m \neq n, \end{aligned} \quad (17)$$

This definition fully controls radiated power optimization and far-field correlation while maximizing total efficiency.

Before showing the described theory in an example, it is worth pointing out the following remarks. The system with  $M$  clusters needs, in total,  $M^2$  constraints<sup>2</sup>. This number becomes considerably high even for a small number of antenna clusters. In practice, however, some constraints might be omitted. For example, the channel correlation between particular clusters can be already sufficiently low due to a geometrical arrangement.

Although the first choice of the power ratios in problem (17) might be  $\alpha_{mm} = 1/M$  and  $\beta_{mn}, \gamma_{mn} \rightarrow 0$ , it is beneficial to perform a sweep over these values. The sweep not only provides an understanding of how radiated power is distributed among the channels, but it might also offer important relaxations that would be compensated by gains in overall performance.

Throughout this paper, the solution of problem (17) is approached using a dual formulation [30] and QCQP solvers contained within the fundamental bounds package [31]. When a duality gap [30] is present, the interior-point method [32] applied directly to the primal problem is utilized instead. In these cases, the localization of a global optimum is not assured. A comparison with the Monte Carlo method suggests that these extremal points might be globally optimal.

### IV. EXAMPLE: PARALLEL DIPOLES

To demonstrate the most salient features of the proposed optimization, four thin parallel dipoles made of a perfect electric conductor are used, see Fig. 2. The length of each strip is equal to  $L = 0.916 c_0 / (2f_0)$ , where  $f_0 = 750$  MHz. Spacing between dipoles is equal to  $L/4$ . All ports are connected to the  $50 \Omega$  transmission line, and no additional components are used for matching. Figure 2 also shows how antenna elements are grouped into two clusters. The in-house method of moments solver [33] is employed for the system analysis.

<sup>2</sup>The given number respects the dependence of power components.

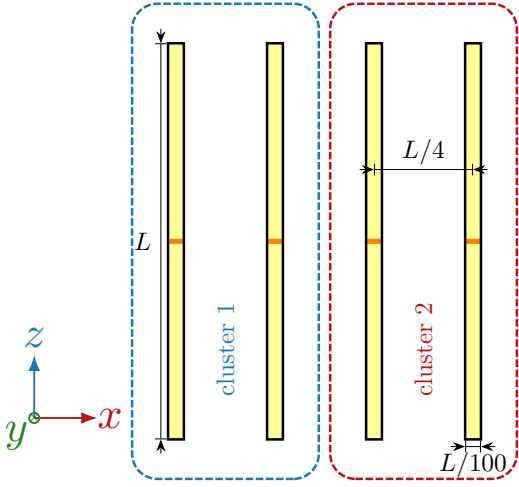


Fig. 2. Illustration of the considered MIMO system. The dimensions are not shown in the correct proportions. The blue and red curves highlight the first and second clusters. All dipoles are fed with delta gaps in places highlighted with orange lines.

The optimization problem reads

$$\begin{aligned} & \underset{\mathbf{v}}{\text{maximize}} && P \\ & \text{subject to} && P_{\text{in}} = 1, \\ & && P_{11} = \alpha_{11}P, \\ & && P_{12,\text{real}} = \beta_{12}P, \\ & && P_{12,\text{imag}} = \gamma_{12}P, \end{aligned} \quad (18)$$

where  $\alpha_{11}$ ,  $\beta_{12}$ , and  $\gamma_{12}$  are swept. In practical scenarios, a given ratio  $\kappa_{12}$  between  $P_{11}$  and  $P_{22}$  is typically of interest. Utilizing the dependence (11) and defining a power ratio  $\kappa_{12}$  as

$$\kappa_{12} = \frac{P_{22}}{P_{11}} = \frac{\alpha_{22}}{\alpha_{11}} \quad (19)$$

allows fixing the power ratio  $\kappa_{12}$  by using

$$\alpha_{11} = \frac{1 - \beta_{12}}{1 + \kappa_{12}}, \quad (20)$$

thereby reducing the sweep to only two dimensions. The rest of this section is dedicated to solving problem (18) on different frequencies with various power ratio settings to show different features of the developed theory.

The results of the two optimization problems are compared: the maximization of total efficiency  $\eta$  in problem (13) and the simultaneous minimization of the envelope correlation coefficient  $E_{12}$  in problem (18). In the latter case, the optimization is solved using  $\kappa_{12} = 1$ ,  $\beta_{12} = 0$  and  $\gamma_{12} = 0$ , *i.e.*, enforcing the zero correlation coefficient and enforcing equal power distribution among the channels. Considering the properties of constrained optimization [30], [32], the expected result is a lower value of total efficiency for constrained problem (18) as compared to the former problem (13). Figure 3 shows that optimization of total efficiency leads to a relatively large envelope correlation coefficient ( $E_{12} > 0.5$ ) in most of the studied frequencies. When the constraint on  $E_{12}$  is added, total efficiency is slightly decreased, but the envelope correlation

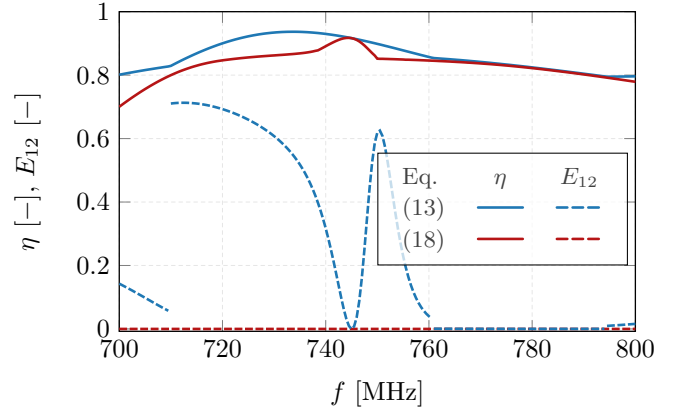


Fig. 3. The frequency sweep of total efficiency  $\eta$  and envelope correlation coefficient  $E_{12}$  for  $\kappa_{12} = 1$ ,  $\beta_{12} = 0$  and  $\gamma_{12} = 0$ . The blue color represents the former optimization problem (13), and the red is its modified version (18). The jump in the blue dashed curve is caused by the change of feeding eigenvector  $\mathbf{v}$  to a different mode.

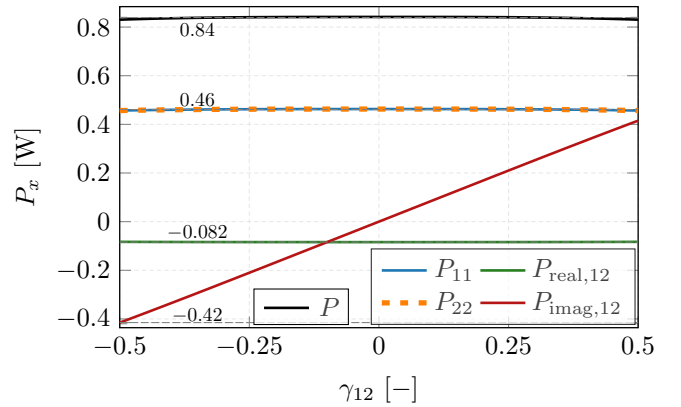


Fig. 4. The sweep of power ratio  $\gamma_{12}$  at  $f = 721$  MHz with  $\beta_{12} = -0.1$ ,  $\alpha_{11} = 0.55$  and  $\alpha_{22} = 0.55$ . The input power reads  $P_{\text{in}} = 1$  W. The black curve denotes total radiated power  $P$ . The rest of the curves depict its decomposition into individual parts (10).

coefficient is kept at zero guaranteeing acceptable MIMO performance.

Various power ratio settings are further studied in Fig. 4 which demonstrates the situation in which problem (18) is solved at  $f = 721$  MHz with  $\kappa_{12} = 1$ ,  $\beta_{12} = -0.1$  and  $\gamma_{12} \in [-0.5, 0.5]$ . It shows how different power components (10) are related to total radiated power  $P$  through power ratios. The curves for  $P_{11}$  and  $P_{22}$  overlay each other as the power ratio reads  $\kappa_{12} = 1$ .

Evaluating the trade-off between total efficiency  $\eta$  and envelope correlation coefficient  $E_{12}$ , the power ratio sweep is extended to  $\beta_{12}, \gamma_{12} \in [-0.5, 0.5]$ , see Fig. 5, and problem (18) is solved at  $f = 735$  MHz with  $\kappa_{12} = 10$ . Total efficiency is depicted as a contour plot and envelope correlation is shown with ellipses of constant  $E_{12}$ , see Appendix C. The figure also shows that not all combinations of power ratios lead to a feasible solution. The unfeasible solutions are bounded by a maximal envelope correlation ellipse. Optimal total efficiency and the optimal envelope correlation coefficient lie at different spots in the  $\beta_{12} \times \gamma_{12}$  space, showing that they are conflicting

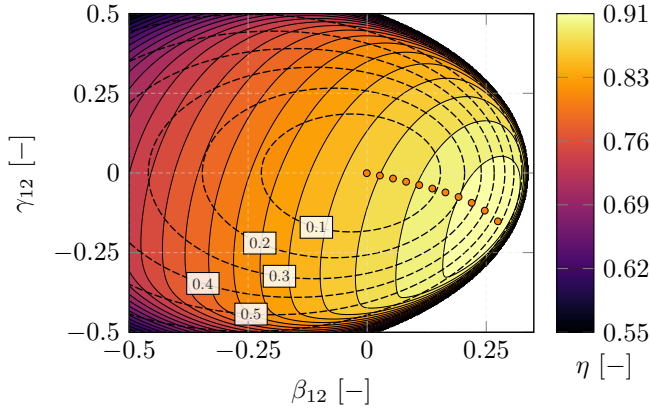


Fig. 5. The power ratio sweep  $\beta_{12} \in [-0.5, 0.5]$  and  $\gamma_{12} \in [-0.5, 0.5]$  for power ratio  $\kappa_{12} = 10$ . The solid-line contour plot depicts total efficiency. Dashed ellipses are regions of constant envelope correlation  $E_{12}$ . The orange dots refer to Pareto-optimal solutions Fig. 6.

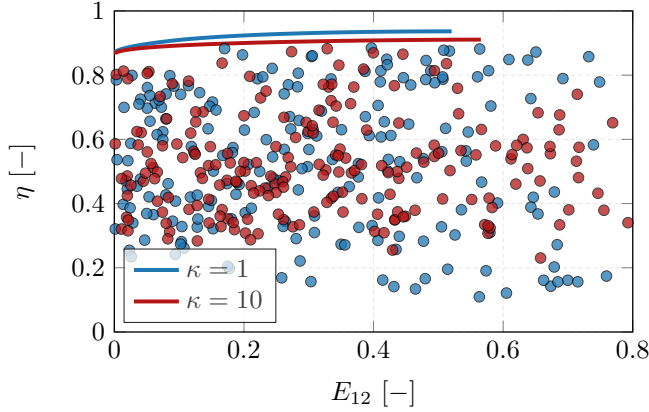


Fig. 6. The trade-off between the envelope correlation coefficient and total efficiency for two different ratios  $\kappa_{12}$  between self powers. Pareto optimal curves are highlighted. Dots represent randomly generated solutions.

parameters.

The trade-off between total efficiency  $\eta$  and envelope correlation coefficient  $E_{12}$  at frequency  $f = 735$  MHz is shown in Fig. 6. The blue and red continuous curves are Pareto optimal solutions. A feeding vector with good efficiency is not a guarantee of an acceptable envelope correlation coefficient. The blue and red dots represent randomly generated solutions fulfilling constraints on input power and power ratio  $\kappa_{12}$ . Random solutions lie under the Pareto frontiers, proving the validity of the presented method. In this specific case, there is only a slight difference in performance between different power ratios  $\kappa_{12}$ . Also, the drop in efficiency for lower envelope correlation coefficients is minor.

The radiation patterns for  $\kappa_{12} = 1$ ,  $\beta = -0.045$  and  $\gamma = 0$ , see Fig. 3, at frequency 750 MHz are depicted in Fig. 7. The pattern of the whole system corresponding to voltage vector  $\mathbf{v} = [\mathbf{v}_1^T \ \mathbf{v}_2^T]^T$  solving problem (18) is depicted in purple. This radiation pattern is composed of individual patterns of each cluster (blue and red), which correspond to voltage vectors  $\mathbf{v} = [\mathbf{v}_1^T \ \mathbf{0}^T]^T$  and  $\mathbf{v} = [\mathbf{0}^T \ \mathbf{v}_2^T]^T$ , respectively, and resemble cardioids with the opposite orien-

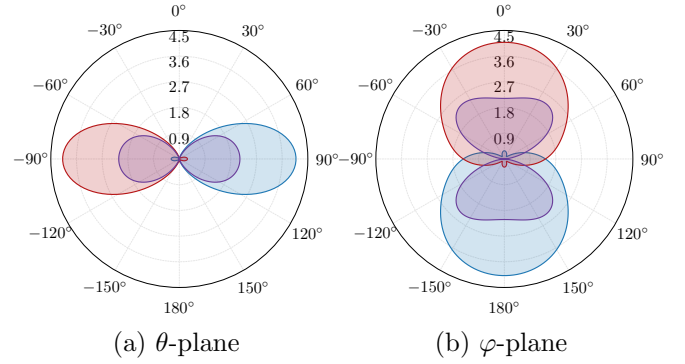


Fig. 7. Total and partial radiation patterns resulting from the solution to (18) for  $\kappa_{12} = 1$ ,  $\beta = -0.045$  and  $\gamma = 0$  at central frequency  $f_0$ . The red and blue colors represent each channel. (a) cut in  $\varphi = 0$ . (b) cut in  $\theta = \pi/2$ .

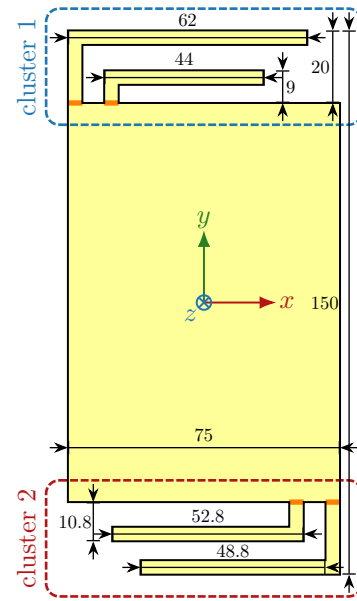


Fig. 8. Simplified model of a mobile terminal. The blue and red curves highlight the first and second clusters. Monopole antennas are fed with delta gaps in places highlighted with orange lines. The dimensions are in millimeters.

tation of their main lobes, a sound solution for high efficiency and low far-field correlation.

## V. EXAMPLE: MOBILE TERMINAL

The second studied structure resembles a mobile terminal introducing a more realistic antenna example with size restricted to common present-day devices, see Fig. 8. The antenna system is considered for operations in the vicinity of 900 MHz. All ports are connected to  $50\ \Omega$  transmission lines and no additional components are used for matching. The presented system is purposely not symmetric. The four antenna elements are grouped into two clusters as indicated in Fig. 8.

Enforcing the vanishing envelope correlation coefficient is, generally, not the best strategy for optimization due to its price in total efficiency. Instead, it is beneficial to add an

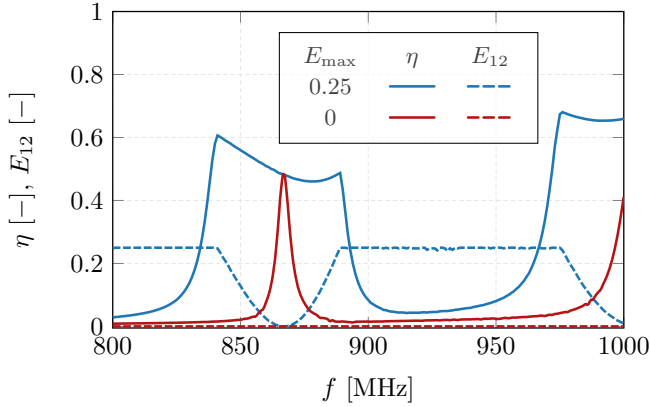


Fig. 9. The frequency sweep of total efficiency  $\eta$  and the envelope correlation coefficient  $E_{12}$  for  $\kappa_{12} = 1$ . The red color represents the optimization problem for  $E_{12} = 0$ , and the blue curve is the problem with envelope correlation coefficient  $E_{12} \leq 0.25$ .

additional non-equality constraint that sets a tolerance for envelope correlation coefficient  $E_{12}$  under a given threshold

$$\begin{aligned}
 & \underset{\mathbf{v}}{\text{maximize}} && P \\
 & \text{subject to} && P_{\text{in}} = 1, \\
 & && P_{11} = \alpha_{11}P, \\
 & && P_{12,\text{real}} = \beta_{12}P, \\
 & && P_{12,\text{imag}} = \gamma_{12}P, \\
 & && E_{12} \leq E_{\text{max}},
 \end{aligned} \tag{21}$$

where  $E_{\text{max}}$  is the maximal allowed envelope correlation coefficient.

Figure 9 shows the solution to problem (21) where the set of red curves corresponds to  $E_{\text{max}} = 0$  and the blue curves represent a solution for  $E_{\text{max}} = 0.25$ . The cost of zero envelope correlation coefficient  $E_{12}$  is a significant drop in total efficiency  $\eta$  in the entire frequency region. Allowing a higher envelope correlation coefficient than zero (always the case in practical applications) leads to substantially better results in total efficiency.

The trade-off between total efficiency  $\eta$  and envelope correlation coefficient  $E_{12}$  is shown in Fig. 10 for  $f = 960$  MHz and for two different power ratios  $\kappa_{12}$ . The maximum allowed value of correlation  $E_{\text{max}}$  is not limited in this case. The continuous lines are Pareto frontiers, while the dots represent randomly generated solutions. This example highlights the conflict between the power ratio and total efficiency caused by the lack of symmetries. Unlike the previous example, this antenna model has a significant trade-off between total efficiency and the envelope correlation coefficient.

The distributed transceiver implementation [24] limits the deployment of antenna cluster technology. Optimal feeding cannot be applied to all frequencies simultaneously due to physical realization restrictions [24], it would have to be discretized into narrower sub-bands. This introduces a trade-off of how many frequency points should be used to conserve a desired performance. Addressing this problem leads to treating the bandwidth of optimal feeding coefficients near a single frequency. Figure 11 shows the difference in performance

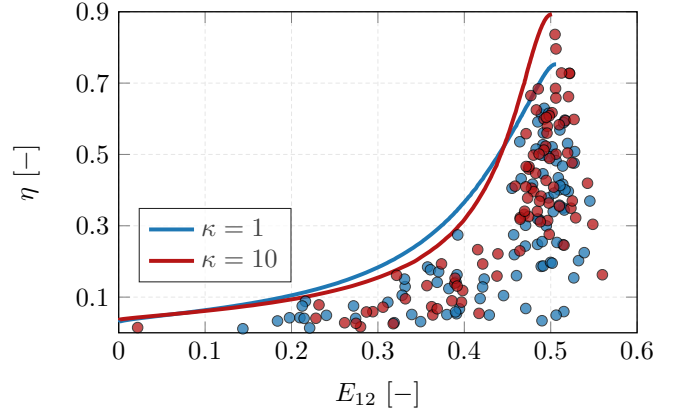


Fig. 10. Trade-off between the envelope correlation coefficient and total efficiency for the mobile terminal model at frequency  $f = 960$  MHz. Two different ratios  $\kappa_{12}$  between powers are shown. The blue and red dots are randomly generated solutions from the Monte Carlo method. Pareto-optimal curves are highlighted by the solid lines.

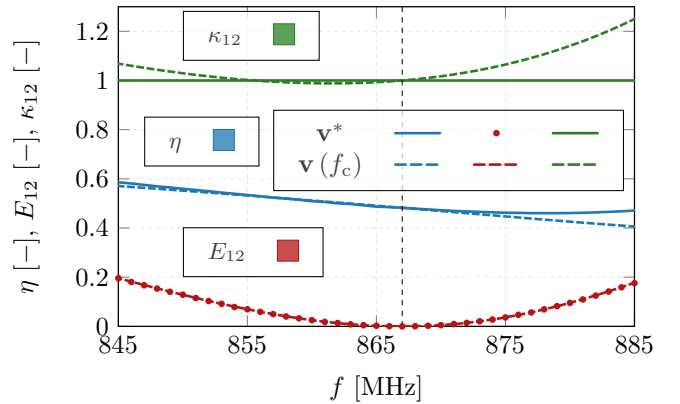


Fig. 11. Comparison of solutions to problem (21) with  $E_{\text{max}} = 0.25$ . Solid lines show the performance of voltage vector  $\mathbf{v}$  optimized at each frequency. Dashed lines correspond to the voltage vector that is only optimal at frequency  $f_c = 867$  MHz (highlighted by the black dashed vertical line).

for the case when the optimal solution to problem (21) is applied to all frequencies in a given sub-band and for the case where the optimal solution for  $f_c = 867$  MHz is applied to all considered frequencies. Total efficiency  $\eta$ , envelope correlation coefficient  $E_{12}$ , and power ratio  $\kappa_{12} = P_{11}/P_{22}$  at  $f_c$  are equal for both excitation schemes. All metrics gradually change as the distance from  $f_c$  increases. To summarize, the optimal voltages do not deviate significantly when the frequency is changed, though the effect of frequency detuning must be evaluated in more detail in the future, also keeping in mind that feeding transmission lines between the feeding circuitry and the antenna port would result in additional dispersion.

## VI. CONCLUSION

The theory of antenna cluster optimization has been expanded toward evaluating the trade-off between total efficiency, envelope correlation coefficients, and power radiated by each cluster. The trade-off is evaluated via a solution to the quadratic optimization problem for maximization of total efficiency extended with the capability to deal simultaneously



with the three mentioned parameters. This is enabled by introducing ratios between the power radiated by the clusters and radiated power component separation. The series of results in the two examples validate the proposed theory with the second example highlighting the trade-off between the three mentioned parameters. The most significant outcome of this paper is to demonstrate the ability of an antenna cluster to balance the level of far-field pattern correlation and total efficiency.

The optimization procedure yields optimal voltages which provide Pareto-optimal performance when connected to the antenna's ports. Applying optimal voltages to all frequencies leads to an unattainable complexity of feeding circuitry. Therefore, the distributed transceiver needs to operate in sub-bands where one solution is applied. The feeding circuitry is also limited to discrete levels of feeding coefficients magnitudes and phases, which can further affect the performance, and with dispersion caused by transmission lines between the distributed transceiver and antenna ports. This work did not assume any form of matching circuits for further total efficiency enhancement. This is an additional set of degrees of freedom to be considered by an antenna designer.

An unresolved issue is the occasional appearance of a duality gap when the dual formulation is employed to solve the optimization problem. The employment of different solving schemes should also be investigated to guarantee a globally optimal solution. This problem will likely be enhanced when more than two antenna clusters are studied. Lastly, the presented investigation raised the question concerning the minimal number of ports required to guarantee the desired performance in all optimized metrics.

#### APPENDIX A MATRIX OPERATORS AND PORT QUANTITIES

The considered radiating system is described by the impedance matrix  $\mathbf{Z} = \mathbf{R}_0 + i\mathbf{X}_0$  extracted from any integral equations [34], [35] method

$$\mathbf{Z}\mathbf{I} = \mathbf{V}, \quad (22)$$

where  $\mathbf{I}$  aggregates current approximation coefficients and  $\mathbf{V}$  is a discrete form of an excitation [36]. The antenna metrics are commonly expressed as linear and quadratic forms of current vector  $\mathbf{I}$ . Notable examples used in this paper are radiated  $P$  and reactive  $P_{\text{react}}$  powers

$$\frac{1}{2}\mathbf{I}^H\mathbf{Z}\mathbf{I} \approx P + iP_{\text{react}}. \quad (23)$$

This paper deals with only lossless structures. However, the losses can be involved by adding loss matrix  $\mathbf{R}_\rho$  into impedance matrix  $\mathbf{Z}$  without any other changes.

Two operators are defined for the purposes of transforming into port modes [26] with the first reading

$$D_{mn} = \begin{cases} \zeta_m & m = n, \\ 0 & \text{otherwise,} \end{cases} \quad (24)$$

where  $\zeta_m$  is a parameter used to control units of port quantities. The second operator is a port indexing matrix defined as

$$N_{mn} = \begin{cases} 1 & \text{the } n\text{-th port is placed at the } m\text{-th position,} \\ 0 & \text{otherwise.} \end{cases} \quad (25)$$

Current vector  $\mathbf{I}$  can now be controlled with voltage sources at antenna ports as

$$\mathbf{I} = \mathbf{Y}\mathbf{D}\mathbf{N}\mathbf{v}, \quad (26)$$

where admittance matrix  $\mathbf{Y}$  is an inverse of the  $\mathbf{Z}$  operator. Relation (26) can be used to transform MoM matrices  $\mathbf{M}$  to their port equivalents

$$\mathbf{m} = \mathbf{N}^H\mathbf{D}^H\mathbf{Y}^H\mathbf{M}\mathbf{Y}\mathbf{D}\mathbf{N}. \quad (27)$$

As an example, relation (27) can be used to transform radiation operator  $\mathbf{R}_0$  from (23) to port radiation matrix

$$\mathbf{g}_0 = \mathbf{N}^H\mathbf{D}^H\mathbf{Y}^H\mathbf{R}_0\mathbf{Y}\mathbf{D}\mathbf{N}, \quad (28)$$

with the help of which the radiated power can be evaluated as

$$P \approx \frac{1}{2}\mathbf{v}^H\mathbf{g}_0\mathbf{v}. \quad (29)$$

Another essential quantity is the power delivered into the radiating system which is used to constrain the optimization problem. Available power [27] can be determined based on the knowledge of the admittance matrix [28] of the feeding system. If the signal generators are uncoupled and connected to the antennas with transmission lines of real-valued impedance, available power is equal to incident power [29], which can be determined as

$$P_{\text{in}} = \frac{1}{2}\mathbf{a}^H\mathbf{a}. \quad (30)$$

To make it suitable for the optimization considered in this paper, incoming power waves  $\mathbf{a}$  are related to port voltages  $\mathbf{v}$  as [26]

$$\mathbf{a} = \mathbf{k}_i\mathbf{v} = \frac{1}{2}(\Lambda^{-1} + \Lambda\mathbf{y}_0)\mathbf{v}. \quad (31)$$

Finally, a combination of (29) and (30) leads to total efficiency [26]

$$\eta = \frac{\mathbf{I}^H\mathbf{R}_0\mathbf{I}}{\mathbf{a}^H\mathbf{a}} = \frac{\mathbf{v}^H\mathbf{g}_0\mathbf{v}}{\mathbf{v}^H\mathbf{k}_i^H\mathbf{k}_i\mathbf{v}}, \quad (32)$$

which is the metric to be maximized in this text.

#### APPENDIX B FAR-FIELD CORRELATION

Mutual radiated power  $P_{mn}$ , typically used to quantify far-field orthogonality, can be evaluated as

$$P_{mn} = \frac{1}{2Z_0} \oint_S \mathbf{F}_m^*(\theta, \varphi) \cdot \mathbf{F}_n(\theta, \varphi) d\Omega, \quad (33)$$

where indices  $m, n$  denote current vectors  $\mathbf{I}_m, \mathbf{I}_n$  excited on an antenna. Utilizing method of moments together with (29), this can be written as a quadratic form

$$P_{mn} = \frac{1}{2}\mathbf{I}_m^H\mathbf{R}_0\mathbf{I}_n = \frac{1}{2}\mathbf{v}_m^H\mathbf{g}_{0, mn}\mathbf{v}_n, \quad (34)$$

with the help of which a far-field correlation coefficient  $\rho_{mn}$  is expressed as

$$\rho_{mn} = \frac{\mathbf{v}_m^H \mathbf{g}_{0,mn} \mathbf{v}_n}{\sqrt{\mathbf{v}_m^H \mathbf{g}_{0,mm} \mathbf{v}_m} \sqrt{\mathbf{v}_n^H \mathbf{g}_{0,nn} \mathbf{v}_n}}. \quad (35)$$

Although the generally complex coefficient (35) is not directly suitable for convex optimization, individual quadratic forms in the nominator and denominator can be added to the optimization problem as additional constraints.

The envelope correlation coefficient  $E_{mn}$  reads

$$E_{mn} \approx |\rho_{mn}|^2. \quad (36)$$

#### APPENDIX C

##### CORRELATION EXPRESSED WITH POWER RATIOS

This section expresses correlation through power ratios. Considering a case of two antenna clusters  $M = 2$ , the far-field correlation coefficient reads

$$\rho_{12} = \frac{\mathbf{v}_1^H \mathbf{g}_{0,12} \mathbf{v}_2}{\sqrt{\mathbf{v}_1^H \mathbf{g}_{0,11} \mathbf{v}_1} \sqrt{\mathbf{v}_2^H \mathbf{g}_{0,22} \mathbf{v}_2}} = \frac{1}{2} \frac{\beta_{12} + i\gamma_{12}}{\sqrt{\alpha_{11}} \sqrt{\alpha_{22}}}, \quad (37)$$

which is obtained by dividing every term  $\mathbf{v}_m^H \mathbf{g}_{0,mn} \mathbf{v}_n$  with  $\mathbf{v}^H \mathbf{g}_0 \mathbf{v}$  and utilizing the power ratios. The ratio between self powers  $\kappa_{12} = P_{11}/P_{22}$  is usually of interest. Using (11) and ratio  $\kappa_{12}$  allows us to express  $\alpha_{11}$  as

$$\alpha_{11} = \frac{1 - \beta_{12}}{1 + \kappa_{12}}, \quad (38)$$

and  $\alpha_{22} = \kappa_{12} \alpha_{11}$ . Putting (38) into relation (37) leads to

$$E_{12} = \left( \frac{1 + \kappa_{12}}{2\sqrt{\kappa_{12}}} \right)^2 \frac{\beta_{12}^2 + \gamma_{12}^2}{(\beta_{12} - 1)^2}. \quad (39)$$

The first term in parentheses in (39) is the scaling factor and the rest of the expression forms the equation for the ellipse. Considering  $\kappa_{12} = 1$  for simplicity, then the expression (39) can be rewritten as

$$\frac{(1 - E_{12})^2}{E_{12}} \left( \beta_{12} + \frac{E_{12}}{1 - E_{12}} \right)^2 + \frac{1 - E_{12}}{E_{12}} \gamma_{12}^2 = 1, \quad (40)$$

which is an ellipse equation. The general  $\kappa_{12}$  would need only a re-scaling of  $E_{12}$  by the factor in parentheses in equation (39).

#### APPENDIX D

##### POWER RATIOS INTERVALS

The radiated power ratios cannot be arbitrary. The feasible intervals for these quantities can be obtained using generalized eigenvalue problems. Starting with self powers, the maximal value of  $\alpha_{mm}$  is found as

$$\tilde{\mathbf{g}}_{0,mm} \mathbf{v}_j = \alpha_j \mathbf{g}_0 \mathbf{v}_j, \quad (41)$$

and the corresponding interval reads  $\alpha \in [0, \max \alpha_j]$ .

A similar approach is used for mutual power ratios. The generalized eigenvalue problems read

$$(\tilde{\mathbf{g}}_{0,mn} + \tilde{\mathbf{g}}_{0,nm}) \mathbf{v}_k = \beta_k \mathbf{g}_0 \mathbf{v}_k, \quad (42)$$

$$i(\tilde{\mathbf{g}}_{0,mn} - \tilde{\mathbf{g}}_{0,nm}) \mathbf{v}_l = \gamma_l \mathbf{g}_0 \mathbf{v}_l, \quad (43)$$

and determine intervals  $\beta_{mn} \in [\min \beta_k, \max \beta_k]$  for the real part and  $\gamma_{mn} \in [\min \gamma_l, \max \gamma_l]$  for the imaginary part of mutual powers.

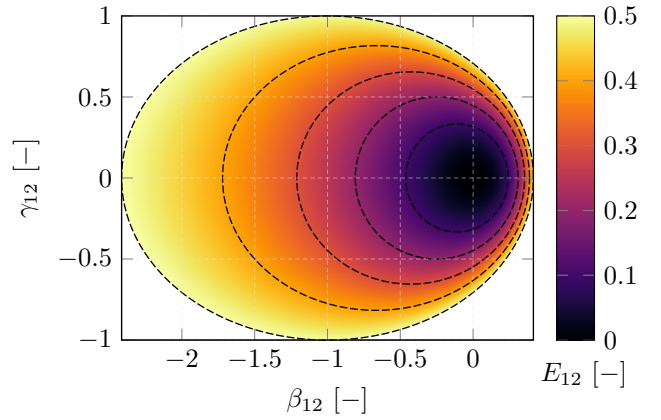


Fig. 12. Depiction of envelope correlation expressed with power ratios for the case of two antenna clusters and  $\kappa_{12} = 1$ . Dashed ellipses show curves of the constant envelope correlation coefficient. Values higher than  $E_{12} > 0.5$  are not shown in compliance with [2].

#### REFERENCES

- [1] A. Paulraj, R. Nabar, and D. Gore, *Introduction to Space-time Wireless Communications*. Cambridge University Press, 2003.
- [2] (2023, Apr.) 3rd Generation Partnership Project (3GPP) . 3GPP. [Online]. Available: <https://www.3gpp.org/>
- [3] M. Giordani, M. Polese, M. Mezzavilla, S. Rangan, and M. Zorzi, "Toward 6G Networks: Use Cases and Technologies," *IEEE Communications Magazine*, vol. 58, no. 3, pp. 55–61, 2020.
- [4] I. F. Akyildiz, A. Kak, and S. Nie, "6G and Beyond: The Future of Wireless Communications Systems," *IEEE Access*, vol. 8, pp. 133 995–134 030, 2020.
- [5] A. Ghasemi, A. Abedi, and F. Ghasemi, *Propagation Engineering in Wireless Communications*, 2nd ed. Springer Cham, Jun. 2018.
- [6] M. Shafi, J. Zhang, H. Tataria, A. F. Molisch, S. Sun, T. S. Rappaport, F. Tufvesson, S. Wu, and K. Kitao, "Microwave vs. Millimeter-Wave Propagation Channels: Key Differences and Impact on 5G Cellular Systems," *IEEE Communications Magazine*, vol. 56, no. 12, pp. 14–20, 2018.
- [7] R. G. Vaughan and J. B. Andersen, "Antenna Diversity in Mobile Communications," *IEEE Transactions on Vehicular Technology*, vol. 36, no. 4, pp. 149–172, 1987.
- [8] C. A. Balanis, *Antenna Theory: Analysis and Design*, 2nd ed. Wiley, 1996.
- [9] S. Kumar, A. S. Dixit, R. R. Malekar, H. D. Raut, and L. K. Shevada, "Fifth Generation Antennas: A Comprehensive Review of Design and Performance Enhancement Techniques," *IEEE Access*, vol. 8, pp. 163 568–163 593, 2020.
- [10] J. Park, M. Jeong, N. Hussain, S. Rhee, S. Park, and N. Kim, "A Low-Profile High-Gain Filtering Antenna for Fifth Generation Systems Based on Nonuniform Metasurface," *Microwave and Optical Technology Letters*, vol. 61, no. 11, pp. 2513–2519, 2019. [Online]. Available: <https://onlinelibrary.wiley.com/doi/abs/10.1002/mop.31931>
- [11] S. Stein, "On Cross Coupling in Multiple-Beam Antennas," *IRE Transactions on Antennas and Propagation*, vol. 10, no. 5, pp. 548–557, 1962.
- [12] S. Blanch, J. Romeu, and I. Corbella, "Exact Presentation of Antenna System Diversity Performance From Input Parameter Description," *Electronics Letters*, vol. 39, pp. 705–707, 06 2003.
- [13] I. Nadeem and D.-Y. Choi, "Study on Mutual Coupling Reduction Technique for MIMO Antennas," *IEEE Access*, vol. 7, pp. 563–586, 2019.
- [14] M. Ayatollahi, Q. Rao, and D. Wang, "A Compact, High Isolation and Wide Bandwidth Antenna Array for Long Term Evolution Wireless Devices," *IEEE Transactions on Antennas and Propagation*, vol. 60, no. 10, pp. 4960–4963, 2012.
- [15] R. A. Bhatti, J.-H. Choi, and S.-O. Park, "Quad-Band MIMO Antenna Array for Portable Wireless Communications Terminals," *IEEE Antennas and Wireless Propagation Letters*, vol. 8, pp. 129–132, 2009.
- [16] C.-Y. Chiu, C.-H. Cheng, R. D. Murch, and C. R. Rowell, "Reduction of Mutual Coupling Between Closely-Packed Antenna Elements," *IEEE Transactions on Antennas and Propagation*, vol. 55, no. 6, pp. 1732–1738, 2007.



- [17] S.-C. Chen, Y.-S. Wang, and S.-J. Chung, "A Decoupling Technique for Increasing the Port Isolation Between Two Strongly Coupled Antennas," *IEEE Transactions on Antennas and Propagation*, vol. 56, no. 12, pp. 3650–3658, 2008.
- [18] R. Martens and D. Manteuffel, "Systematic Design Method of a Mobile Multiple Antenna System Using the Theory of Characteristic Modes," *IET Microwaves, Antennas Propagation*, vol. 8, no. 12, pp. 887–893, 2014.
- [19] B. Yang and J. J. Adams, "Systematic Shape Optimization of Symmetric MIMO Antennas Using Characteristic Modes," *IEEE Transactions on Antennas and Propagation*, vol. 64, no. 7, pp. 2668–2678, 2016.
- [20] R. Martens and D. Manteuffel, "2-port Antenna Based on the Selective Excitation of Characteristic Modes," in *Proceedings of the 2012 IEEE International Symposium on Antennas and Propagation*, 2012, pp. 1–2.
- [21] N. Peitzmeier and D. Manteuffel, "Upper Bounds and Design Guidelines for Realizing Uncorrelated Ports on Multimode Antennas Based on Symmetry Analysis of Characteristic Modes," *IEEE Transactions on Antennas and Propagation*, vol. 67, no. 6, pp. 3902–3914, 2019.
- [22] M. Masek, L. Jelinek, and M. Capek, "Excitation of Orthogonal Radiation States," *IEEE Transactions on Antennas and Propagation*, vol. 69, no. 9, pp. 5365–5376, 2021.
- [23] J. M. Hannula, T. Saarinen, J. Holopainen, and V. Viikari, "Frequency Reconfigurable Multiband Handset Antenna Based on a Multichannel Transceiver," *IEEE Transactions on Antennas and Propagation*, vol. 65, no. 9, pp. 4452–4460, 2017.
- [24] A. R. Saleem, K. Stadius, J.-M. Hannula, A. Lehtovuori, M. Kosunen, V. Viikari, and J. Ryyänen, "A 1.5–5-GHz Integrated RF Transmitter Front End for Active Matching of an Antenna Cluster," *IEEE Transactions on Microwave Theory and Techniques*, vol. 68, no. 11, pp. 4728–4739, 2020.
- [25] J.-M. Hannula, T. Saarinen, A. Lehtovuori, J. Holopainen, and V. Viikari, "Tunable Eight-Element MIMO Antenna Based on the Antenna Cluster Concept," *IET Microwaves, Antennas and Propagation*, vol. 13, Feb. 2019.
- [26] M. Capek, L. Jelinek, and M. Masek, "Finding Optimal Total Active Reflection Coefficient and Realized Gain for Multiport Lossy Antennas," *IEEE Transactions on Antennas and Propagation*, vol. 69, no. 5, pp. 2481–2493, 2021.
- [27] C. Desoer, "The Maximum Power Transfer Theorem for N-ports," *IEEE Transactions on Circuit Theory*, vol. 20, no. 3, pp. 328–330, 1973.
- [28] F. Broydé and E. Clavelier, "The Radiation and Transducer Efficiencies of a Multiport Antenna Array," *Excem Res. Papers in Electron. and Electromagn.*, no. 4, pp. 1–22, Jan. 2022. [Online]. Available: <https://doi.org/10.5281/zenodo.5816837>
- [29] D. M. Pozar, *Microwave Engineering*, 3rd ed. Wiley, 2005.
- [30] S. Boyd and L. Vandenberghe, *Convex Optimization*. Cambridge University Press, 2004.
- [31] J. Liska, L. Jelinek, and M. Capek, "Fundamental Bounds to Time-Harmonic Quadratic Metrics in Electromagnetism: Overview and Implementation," 2021.
- [32] J. Nocedal and S. Wright, *Numerical Optimization*, 2nd ed., ser. Springer series in operations research. Springer, 2006.
- [33] (2023, Apr.) Antenna Toolbox for MATLAB (AToM). Czech Technical University in Prague. [Online]. Available: [www.antennatoolbox.com](http://www.antennatoolbox.com)
- [34] J. L. Volakis and K. Sertel, *Integral Equation Methods for Electromagnetics*. SciTech Publishing, 2012.
- [35] W. C. Chew, M. S. Tong, and B. Hu, *Integral Equation Methods for Electromagnetic and Elastic Waves*, 1st ed., ser. Synthesis Lectures on Computational Electromagnetics. Morgan and Claypool Publishers, 2007.
- [36] R. F. Harrington, *Field Computation by Moment Methods*, ser. The IEEE PRESS Series in Electromagnetic Waves (Donald G. Dudley, Editor). Wiley-IEEE Press, 1993.